

SLOPE DETECTOR FOR DETERMINATION OF THE RINGING ARTIFACT IN FILTERING X-RAY IMAGES

Dong Sik Kim¹ and Sanggyun Lee²

¹Department of Electronics Engineering, Hankuk University of Foreign Studies
Gyunggi-do, 449-791, Korea, dskim@hufs.ac.kr

²R&D Center, DRTECH Co., Korea

ABSTRACT

In order to reduce the grid artifacts, which are caused by using the antiscatter grid in obtaining x-ray digital images, we analyze the effect of applying band-rejection filters (BRFs) in the frequency domain. The property of the grid artifacts is quite different depending on the shape of the object to be recovered in the spatial domain. Furthermore, if the frequency component of the grid artifact is relatively close to that of the object, then simply applying a BRF may seriously distort the object and cause the ringing artifact. In this paper, we propose a hybrid filtering scheme, which can cooperate such different properties in the spatial domain. In order to perform a robust detection of the position of the ringing artifact, we propose the frequency-modulation (FM) model for the extracted signal, which corresponds to a specific grid artifact. An estimation of the position image for the ringing artifact is then conducted based on the slope detection algorithm, which is commonly used as an FM discriminator in the communication area. Numerical result for real x-ray images shows that applying BRFs in the frequency domain in conjunction with the spatial property of the ringing artifact can successfully remove the grid artifact, distorting the object less.

Index Terms— Frequency modulation model, grid artifacts, slope detector, radiography

1. INTRODUCTION

In x-ray imaging, the radiated x-ray emitted from the source penetrates specimens, and the primary beam reaches the image detector, where digital images are constructed. However, the scattered beam, which is inevitably produced when a primary beam passes through a subject, degrades the image quality. In order to remove undesired scattered beams, an antiscatter grid before the image detector is normally used. The grid is composed of strips, which are made of an x-ray transmitting material, such as aluminum, and an x-ray absorbing material, such as lead. The transmitting and absorbing strips are arranged to the primary radiation, and protect from blurring.

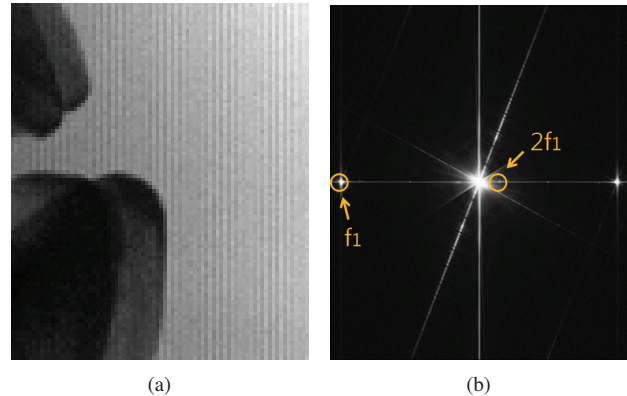


Fig. 1. X-ray image by using the motor grid. (a) Part of image ($\times 32$ magnified). (b) Centers of the grid artifacts from f_1 and $2f_1$ in the frequency domain (the alias of $2f_1$ is very close to the origin, where $139\mu\text{m}/\text{pixel}$ and $103\text{ls}/\text{inch}$).

As high-resolution imaging systems are developed however, *grid artifacts*, which are caused by the grid pattern, become annoyingly visible. In order to remove the grid artifacts, moving grids, which is operated by the spring or motor, are generally employed with additional implementation complexity. Even though we use the moving grids, the grid artifact is still visible as shown in Fig. 1(a), and thus it should be removed from the obtained x-ray image by applying filters in the spatial [1] or frequency domain [2]. In the frequency domain, the grid artifacts can be described as amplitude-modulated terms [3], and thus the band-rejection filters (BRFs) should be applied to remove the grid artifacts. Since the spectrum of the object is usually concentrated around low-frequency area, we can efficiently remove the modulated terms if their locations are as far as possible from the origin. The rotated grid with an appropriate angle for given sampling and grid frequencies can move the locations of the modulated terms to the boundaries in the frequency domain [3]. Instead of the rotated grid, if we use a non-rotated grid, then the modulated terms from the harmonics of the grid frequency occasionally occur near the origin (see ' $2f_1$ ' in Fig. 1(b)). Thus, applying BRFs to these modulated terms may seriously distort the object to be recovered. In order to

minimize the damage to the object, we may apply a narrow bandwidth BRF. The *ringing artifact* is however observed near edges. Here, the ringing artifact occurs when the signal is bandlimited by filtering and is ripples in the sinc function. If we apply a wide bandwidth BRF, of which shape is the Gaussian function, then the reconstructed object is usually blurred. In this paper, we first propose an algorithm to detect the ringing artifacts based on a *frequency-modulation (FM) model* and then develop a hybrid filtering technique in the frequency domain considering the detected artifact in the spatial domain.

2. FILTERING ARTIFACTS IN THE SPATIAL DOMAIN

2.1. Modulation Image Formation Model

For a model of the stationary linear grid, we consider a rectangular signal as $g : \mathbb{R}^2 \rightarrow \{0, 1\}$. The grid image, which is not rotated, is then defined as $g(x, y) = 1$ for $0 \leq x < \tau$, $g(x, y) = 0$ for $\tau \leq x < T$, and $g(x, y) = g(x + T, y)$, for $x, y \in \mathbb{R}$. Here, τ and $T - \tau$ imply the interspacer thickness and the absorber thickness, respectively. The *grid density* or *grid frequency*, which is the number of lead strips per mm, is given by $f_1 := 1/T$ (1s/mm). Since g is periodic with respect to T , g can be expanded as the Fourier series $g(x, y) = a_0 + \sum_{n=1}^{\infty} a_n \cos(2\pi n f_1 x + \theta_n)$, where $n f_1$, for $n = 2, 3, \dots$, are the harmonic frequencies, θ_n are constants, $a_0 = \tau/T$ is the ideal primary radiation of grid, and $a_n = (n\pi)^{-1} \sin(n\pi\tau/T)$, for $n = 1, 2, \dots$. For the analysis of the observed image h_g after the grid, the *modulation image formation model* [3] is defined by a multiplicative form as $h_g(x, y) = h(x, y) \cdot g(x, y)$. Here, a map $h : \mathbb{R}^2 \rightarrow [0, 1]$ represents the original projected image to be recovered, and h_g is an observed image, which can be expanded as

$$\begin{aligned} h_g(x, y) &= a_0 h(x, y) + \sum_{n=1}^{\infty} a_n h(x, y) \cos(2\pi n f_1 x + \theta_n) \quad (1) \end{aligned}$$

for $(x, y) \in \Lambda$. The modulation model of (1) for h_g is a linear combination of the object $h(x, y)$ and the *modulated terms* $h(x, y) \cos(2\pi n f_1 x + \theta_n)$ with the carrier frequencies $n f_1$, $\forall n^1$. Note that the aliases of the modulated terms appear as the grid artifacts and should be removed by using appropriate filters, such as the BRF in the frequency domain.

Let ε_n denote the signal that is removed by the n th BRF. If the spectra of the object h and the modulated terms of $n f_1$, $\forall n$, are not overlapped, then by using an ideal BRF we may successfully extract the modulated terms that cause the grid artifacts. In other words, the extracted signals ε_n satisfy

$$\varepsilon_n \approx a_n h(x, y) \cos(2\pi n f_1 x + \theta_n), \forall n \quad (2)$$

¹An extended model, which can cope with the saturation property, is introduced in [4] to perform the adaptation to the different artifact strengths.

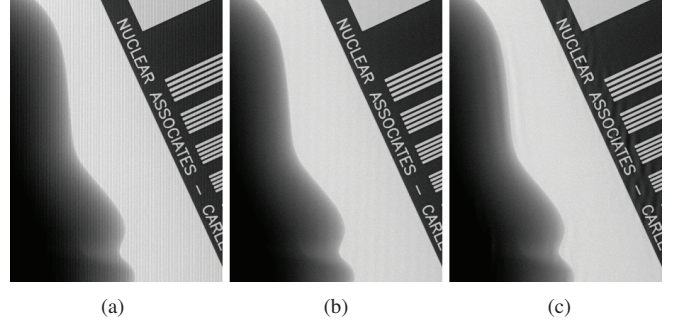


Fig. 2. Adaptive grid artifact rejection based on BRF in the frequency domain [4]. (a) Part of the observed image h_g with the grid artifacts from both f_1 and $2f_1$. (b) Grid artifact from the harmonic frequency $2f_1$ is visible when only the modulated term of f_1 is removed. (c) The ringing artifact is visible around the edge areas when both modulated terms of f_1 and $2f_1$ are removed.

where η_n is the minimal alias frequency of the n th harmonic $n f_1$ and can be calculated by the integer transform function as in [3]. Note that even for the overlap case, the center frequency of the modulated term from $n f_1$, i.e., η_n , should be as far as possible from the origin such that the overlap is minimized. When we extract the n th modulated term by using a BRF in the frequency domain, if η_n is relatively close to the object h . The extracted signal ε_n then may contain a part of h as well as $a_n h(x, y) \cos(2\pi \eta_n x + \theta_n)$. In other words, applying a BRF filter also distorts the recovered image. Furthermore, the extracted signal yields the ringing artifact due to the bandlimited property.

2.2. Example of the Ringing Artifacts

In this section, we analyze the effect of filtering in the frequency domain to the spatial domain by showing an example. To obtain images, we use a direct radiography image detector (DRTECH Co.), of which sampling frequency is $f_s = 7.194$ (139 μ m/pixel) and the grid frequency is $f_1 = 4.055$ (103 1s/inch). The center frequency of the alias of the modulated term from f_1 is $(|f_s - f_1|, 0) = (3.139, 0)$ and is relatively far from the origin $(0, 0)$ in the frequency domain, since the maximum frequency in each axis is given by $|f_s|/2 = 3.597$. Hence, we can successfully remove the modulated term without distorting the object. However, the center frequency of the modulated term from the second harmonic $2f_1$ is given by $(|f_s - 2f_1|, 0) = (0.916, 0)$, which is quite close to the origin as shown in Fig. 1(b). Hence, removing this modulated term may distort the object. In Fig. 2, an example of grid artifact reduction is shown, where a BRF algorithm is employed [4]. Fig. 2(a) is an observed image h_g , which includes the grid artifacts. Fig. 2(b) shows a filtered image, where an adaptive BRF to the artifact strength is applied to the frequency of the modulated term from f_1 . We can notice that the serious grid

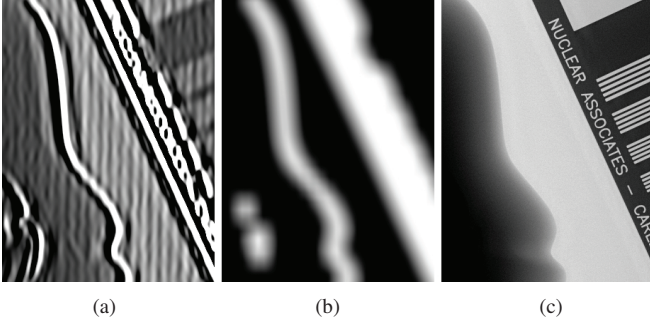


Fig. 3. Hybrid filtering based on the magnitude of $|\varepsilon_n|$. (c) Image of the magnitude $200 \times |\varepsilon_2|$ (5th-order Butterworth BRF with the bandwidth 0.4). (b) Segmented image based on $|\varepsilon_2| > 0.005$, morphological dilation, and then low-pass filtered. (c) Hybrid filtered image result.

artifact from f_1 is removed, but the grid artifact from $2f_1$ is still visible especially in the background area of Fig. 2(b). In Fig. 2(c), BRFs for both the modulated terms from f_1 and $2f_1$ are applied. However, we can notice the annoying ringing artifact near the edge between the skull and background, and around the letters. We can also notice that the edge part is blurred.

2.3. Ringing Artifact Detection Based on $|\varepsilon_n|$

The extracted signal, which is obtained by the BRF for $2f_1$, corresponds to the difference image between the images of Figs. 2(b) and (c), and is shown in Fig. 3(a). Let Figs. 2(b) and (c) be denoted as h_g^1 and h_g^2 , respectively, and Fig. 3(a) be denoted as ε_2 . Then $\varepsilon_2 \approx h_g^1 - h_g^2$ holds. From ε_n , we can also observe the grid artifact, of which alias frequency is $(0.916, 0)$ in the background. However, near the edge areas, seriously distorted signals, which is far from the usual grid artifact, are observed. Since this distortion is dependent on the shape of the object in the spatial domain, an adaptive scheme, which can detect the distorted parts in the spatial domain and then process them in a different way, should be developed.

The region, which shows the ringing artifact, usually have large values of $|\varepsilon_n|$ as shown in Fig. 2(c) and Fig. 3(a). Thus, by searching relatively large $|\varepsilon_n|$ for each pixel $(x, y) \in \Lambda$, we may determine the positions of the ringing artifact. Fig. 3(b) is obtained by thresholding $|\varepsilon_n|$ with a constant T and applying morphological dilation and moving average, where the white part implies the position of the ringing artifact. The final result of the hybrid filtering result based on the magnitude of $|\varepsilon_n|$ is shown in Fig. 3(c). The final image is a linear combination of the filtered images h_g^1 and h_g^2 , and the coefficient is given by the image of Fig. 3(b). In other words, letting $s \subset [0, 1]$ denote the detection image as Fig. 3(b), the filtered image Fig. 3(c) is obtained from

$$h_g^1(x, y) + [1 - s(x, y)] \cdot h_g^2(x, y), \text{ for } (x, y) \in \Lambda. \quad (3)$$

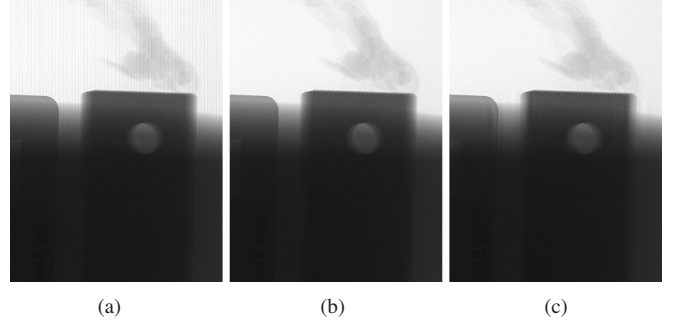


Fig. 4. Other part of the simulation in Fig. 3 (detection is failed due to the low $|\varepsilon_n|$ and low-amplitude ringing artifacts are visible inside the object).

From Fig. 3(c), we can notice that the proposed hybrid method, which is based on the magnitude $|\varepsilon_n|$, can successfully remove the grid artifact from $2f_1$, and the ringing artifact is not visible compared to the usual case of Fig. 2(c). However, the pixels that even show relatively low magnitude of $|\varepsilon_n|$ could belong to the ringing artifact area especially when the pixels of the ringing artifact are inside the object as shown in Fig. 4(c). Instead of using the magnitude of $|\varepsilon_n|$, we consider an FM model for ε_n to describe the ringing artifact and propose a ringing artifact detector, which is based on a discriminator for FM [5]. Note that the FM model is robust to the noisy amplitude compared to the magnitude $|\varepsilon_n|$ case.

3. SLOPE DETECTOR BASED ON THE FREQUENCY MODULATION MODEL

We now propose an FM model for the extracted signal ε_n . Suppose that $p_n(x, y)$ denotes modulating signal for $n f_1$ and its derivative $r_n := \partial p_n / \partial x$ denotes an image that indicates the positions of the ringing artifact that is made by applying a BRF for the modulated term of $n f_1$. Before applying the FM demodulation, a limiter and then a BRF with the center frequency η_n are used to eliminate any amplitude noise present in ε_n [5]. Let ε'_n denote such a signal, which is passed through the limiter and the band-pass filter (BPF). The FM model of the ringing artifact for the extracted signal ε_n is then given by

$$\varepsilon'_n(x, y) := \cos(2\pi\eta_n x + p_n(x, y)), \text{ for } (x, y) \in \Lambda. \quad (4)$$

Here, we set the amplitude as one to simplify the expansion of the FM demodulator. Figs. 5(a) and (b) are limited and BPF images, respectively. As shown in Figs. 5(a) and (b), phase shifts around the ringing artifact area are noticeable. Based on the model of (4), searching the positions of the ringing artifact is to estimate r_n . The estimation of r_n is the demodulation of the FM signal ε'_n [5]. By differentiating ε'_n with respect to x ,

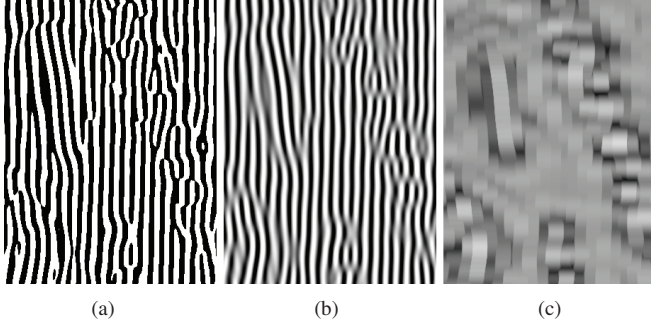


Fig. 5. Slope detection based on the FM model (same part of Fig. 2). (a) Limited image of ε_2 (5th-order Butterworth BRF with the bandwidth 0.2). (b) BPF image of the limited image. (c) Differentiated and then envelop-detected image.

we first obtain

$$\begin{aligned} \frac{\partial \varepsilon'_n(x, y)}{\partial x} &= \left[2\pi\eta_n + \frac{\partial p_n(x, y)}{\partial x} \right] \sin(2\pi\eta_n x + p_n(x, y)) \end{aligned}$$

for $(x, y) \in \Lambda$. If the amplitude term satisfies $2\pi\eta_n + \partial p_n(x, y)/\partial x \geq 0$, then by applying an envelope detector we can extract the amplitude term (see Fig. 5(c)). Finally, we obtain an estimate of $r_n(x, y) = \partial p_n(x, y)/\partial x$ by applying a DC blocking filter to remove $2\pi\eta_n$ (see Fig. 6(a)). By using the estimate of r_n , we segment it based on the Otsu method (see Fig. 6(b)) and obtain a filtered image in a similar manner as (3). For the same part of Fig. 4, Fig. 7 shows the proposed hybrid method, which is based on the FM model. As shown in Fig. 7(b), even though the magnitude of $|\varepsilon_2|$ is relatively small, the slope detector can determine the area as the ringing artifact area. Hence, the hybrid filtered result of Fig. 7(c) does not suffer the ringing artifact problem.

4. CONCLUSION

The property of the grid artifacts is quite different depending on the shape of the object to be recovered in the spatial domain. Furthermore, if the frequency component of the grid artifact in x-ray imaging is relatively close to that of the object, then simply applying a band-rejection filter (BRF) may seriously distort the object, and cause the ringing artifact or blurring. In order to detect the position of the ringing artifact, we proposed the frequency-modulation (FM) model for extracted modulated terms and used the slope detection algorithm, which is usually used as the FM discriminator. Numerical result showed that applying BRFs in the frequency domain with the information on the ringing artifact can successfully remove the grid artifact distorting the original image less. Furthermore, the slope detector can successfully extract the ringing artifact information independently of the magnitude of the ringing artifact.

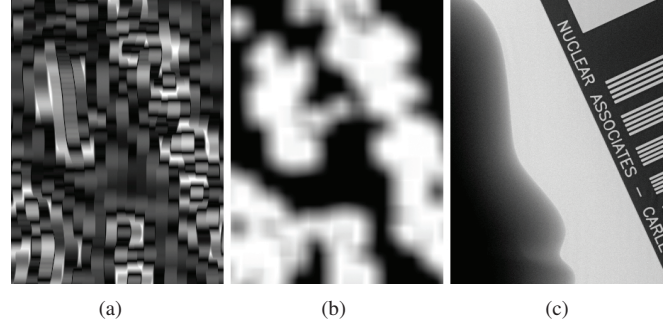


Fig. 6. Proposed hybrid filtering based on the FM model. (a) Mean-extracted image from the envelop-detected image. (b) Segmented image based on the Otsu algorithm, morphological dilation, and then low-pass filtered. (c) Hybrid filtered image result.

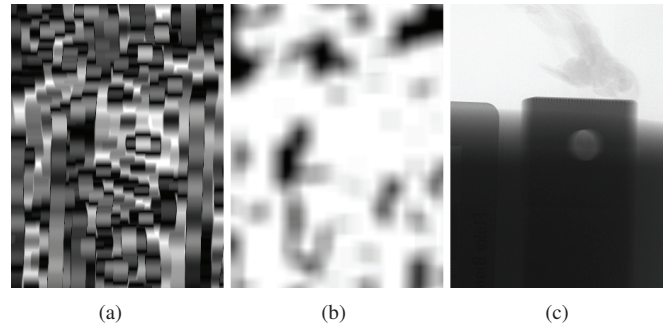


Fig. 7. Other part of the simulation in Fig. 6

5. REFERENCES

- [1] L. L. Barski and X. Wang, "Characterization, detection and suppression of stationary grids in digital projection radiography imagery," in *Proc. SPIE, Image Display*, Feb. 1999, vol. 3658, pp. 502–519.
- [2] C. Y. Lin, W. J. Lee, S. J. Chen, C. H. Tsai, J. H. Lee, Chang C. H., and Y. T. Ching, "A study of grid artifacts formation and elimination in computed radiographic images," *Jour. Digital Imaging*, vol. 19, no. 4, pp. 351–361, Dec. 2006.
- [3] D. S. Kim and S. Lee, "Optimization of the grid frequencies and angles in digital radiography imaging," in *Proc. SPIE, Medical Imaging: Physics of Medical Imaging*, Feb. 2011, vol. 7961, pp. 1957–1960.
- [4] D. S. Kim and S. Lee, "Adaptive grid pattern artifact reduction in radiography imaging based on the significant-signal bandwidth," in *Proc. IEEE Int. Conf. Image Processing*, Sep. 2011, pp. 1505–1508.
- [5] H. P. E. Stern and S. A. Mahmoud, *Communication Systems: Analysis and Design*, Pearson Prentice Hall, NJ, 1st edition, 2004.